AGRONOMY & SOILS

Estimating Cotton Canopy Temperature Artifacts in UAV-Based Thermal Measurements

Timothy S. Goebel*, Andrew Young, Paxton Payton, Murilo Maeda,
Robert J. Lascano, and James R. Mahan

ABSTRACT

Thermal sensors mounted on unmanned aerial vehicles (UAVs) have been used for crop evaluation. The assembly of multiple UAV images into a composite orthomosaic image that represents an agricultural field is common. The creation of these composite orthomosaic images is predicated on the assumption that the variable of interest, for example, plant height, does not change in the interval between the first image and the last image. Canopy temperature is continuously variable. Thus, in a composite thermal image, the temperature differences between any two points can include both the temperature differences of the two locations, as well as the temperature change occurring during the time the images were captured. A modeling approach was used to investigate these temporal thermal artifacts in cotton (*Gossypium hirsutum* L.*)*. The objectives were to analyze the average amount of thermal variation that can occur across a field, identify times of maximum variation, and examine the magnitude of these thermal artifacts across the temporal scale of a typical drone mission. As the time between the first image and last image increased from 15 minutes to an hour, the temporal thermal distortion increased from 0.7 to 1.4 °C for a high-water treatment and from 0.9 to 2.8 °C for a low-water treatment. The simulated flights from 1030 to 1230 h had the largest variation and the 1230 to 1430 h and 1430 to 1630 h flights had less thermal variation. Depending on the application, the thermal distortion could range from negligible to potentially significant.

T.S. Goebel*, A. Young, P. Payton, and J.R. Mahan, USDA-ARS Plant Stress & Germplasm Development Unit, 3810 4th St., Lubbock, TX 79415; M. Maeda, Texas A&M Dept. of Soil & Crop Sciences, 1102 East FM 1294, Lubbock, TX 79403; and R.J. Lascano, USDA-ARS Wind Erosion & Water Conservation Unit, 3810 4th St., Lubbock, TX 79415.
*Corresponding author: tim.goebel@usda.gov

Plant canopy temperature (Tc) is often used as an indicator of plant water status and metabolic optimality (Mahan et al., 2005, 2010; Wanjura and Mahan, 1994; Wanjura et al., 1995, 2002, 2006). In production settings where Tc is used for irrigation control, temperature is most often measured by fixed-position infrared thermometers (Mahan et al., 2005, 2010; Wanjura et al., 1995). Recently, thermal cameras mounted on unmanned aerial vehicles (UAVs), have been used to evaluate larger portions of a field as they have a larger field of view (FOV) compared to fixed-position sensors (Berni et al., 2009a, 2009b; Gonzalez-Dugo et al., 2013; Vadivambal et al., 2011; Zarco-Tejada et al., 2012). Further, the use of UAVs in agriculture has increased during the past few years with various devices deployed in agricultural settings to collect crop data on a larger spatial scale than is practical with in-field fixed-position sensors (Andrade-Sanchez et al., 2014; Pabuayon-Irish et al., 2019; Pratap et al., 2015). The FOV of UAV-mounted sensors can approach production field scales (Chang et al., 2020; Jung et al., 2018).

Photogrammetric approaches have proven useful, and a variety of cameras and sensors can be used to acquire information about crops in fields (Colomina and Molina, 2014; Raeva et al., 2018; Weiss et al., 2020; Zhang and Kovacs, 2012). Photogrammetric approaches are often based on assembling a series of images collected over a desired ground area into a single, orthomosaic image that allows for spatial analysis of objects in the image (Chu et al., 2018; Zhang and Kovacs, 2012). Typical uses include phenology, crop biomass, and harvest index (Gil-Docampo et al., 2020; Walter et al., 2018); crop ground cover (Gerbermann et al., 1976; Roth and Streit, 2018); crop canopy height (Matese et al., 2017; Murakami et al., 2012); and leaf color (Bacsa et al., 2019; Dandois et al., 2017).

A key assumption in measuring crop status (e.g., height, leaf area) with agronomic photogrammetry is that the measured variable does not change during the time required for its measurement. This assumption is undoubtedly valid for individual images, which are acquired in a fraction of a second. Large areas require the capture of multiple images over time. These images are often combined to produce a composite orthomosaic image where the variable is assumed to vary only

with location. However, the time required to collect the individual images can extend from minutes to hours; thus crop variables that change significantly during this time period represent a potential source of measurement error. Such errors will be present in an orthomosaic image that commingles variability in both time and location. An example of this is the measurement of Tc, which changes continuously over the course of the day (Wanjura and Mahan, 1994; Wanjura et al., 2002, 2006).

In-field Tc measurement via fixed-position sensors is often carried out in relatively short time intervals resulting in near continuous profiles of diurnal plant water status over seasonal periods (Mahan et al., 2010; Wanjura et al., 2006). However, a major limitation is that the spatial resolution is relatively small; the FOV for fixed-position sensors is often less than 1 m^2. The ability to attach a thermal sensor to a UAV provides the opportunity to obtain thermal orthomosaic images of relatively large collections of plants within a field. Conversely, the primary limiting factor of photogrammetric approaches to the measurement of Tc is that, unlike plant height or leaf area, Tc is not constant over a daily time period, thus the temporal resolution of aerial Tc must be relatively low. Canopy temperature changes diurnally in response to changing environmental (e.g., air temperature, water availability, and solar radiation) and plant physiological conditions (e.g., transpiration) and thus the change of Tc over the course of a daily UAV mission can result in thermal artifacts when acquired with UAV-based thermal sensors.

A typical agricultural UAV mission often involves the collection of multiple images with each image having its own location (latitude and longitude) and timestamp. The location associated with an image is known and used to create the orthomosaic images that generate unintended spatial variation in the measured variable. The timestamp of each image, although known explicitly, is not used in the creation of the orthomosaic image. Thus, the orthomosaic image developed using multiple thermal images can contain thermal artifacts that result from the diurnal pattern of Tc among the individual images collected during the measurement period. Therefore, the objective of this study was to investigate the sources and quantify the magnitude of time-related thermal artifacts that are possible in orthomosaic thermal images obtained from a typical UAV thermal mission.

MATERIALS AND METHODS

Overview of Approach. The goal of this study was to evaluate the changes in Tc occurring between the first and last thermal images captured during a UAV thermal mission in an agricultural setting. The experiments were conducted at the U.S. Department of Agriculture–Agricultural Research Service, Cropping Systems Research Laboratory in Lubbock, TX (33.59° N, 101.89° W and average elevation of 960 m above sea level).

This study explored the potential for distortion of measured Tc that results from the period between measurements that is inherent in at least some UAV-thermal methods. The approach was to collect a dataset of Tc from a field study and then temporally distort the data to introduce variation in timestamps to represent the temporal variation that would be present in UAV thermal measurements. Because temporal distortion is the only variable generated in the analysis, the time series Tc data required could be collected with any sensor platform as long as the timestamp of the measurement is known. We chose to use fixed-infrared-thermometer (IRT) sensors in the plots to collect Tc data in part because they allowed us to collect Tc data 24 h d^{-1} during the study period in an automated manner. The method was applied to Tc collected in three irrigation treatments.

For the purpose of this study the term sensor image refers to a single image captured by the sensor, and the term orthomosaic image refers to a collection of single images.

Canopy Temperature Measurements. Cotton (*Gossypium hirsutum* L.) (FiberMax 989, BASF Corporation, Florham Park, NJ) was planted on 7 June 2020 at a seeding rate of 12 seeds m^{-1} and 1-m row spacing. Seventy-five mm of irrigation was applied to the field via sub-surface drip 1 wk prior to planting and the field received a total of 66 mm of rain between planting and harvest. Three irrigation treatments were established: 1) low = no in-season irrigation, rainfall only; 2) medium = 109-mm in-season irrigation; 3) high = 284-mm in-season irrigation. The total for each treatment including pre-plant irrigation, in-season rainfall, and in-season irrigation was 150, 275, and 425 mm for the low, medium, and high irrigation treatments, respectively. Measured cotton lint yields in the treatments were 719, 1,230, and 2,456 kg ha^{-1}.

A single IRT (GoField™, GoannaAg, Goondiwindi, QLD, Australia) was installed in each water level 5 wk after emergence. Sensors were positioned 25 cm above the canopy at an angle of approximately 45°. Sensors were repositioned weekly as canopy height increased. Temperature values were compared with blackbody targets twice during the season. The IRT in each plot monitored the cotton Tc in an area of approximately 400 cm^2.

This arrangement of IRTs resulted in three datasets of near-continuous Tc (15-min averages of three measurements at 5-min intervals) for a period of 60 d. Measured Tc used in our analysis were limited to a 60-d period from 25 July 2020 (50 d after planting [DAP]) to 15 September 2020 (110 DAP). The analysis was limited to the daily period when a UAV would normally be flown to collect Tc data. Canopy temperature data were filtered to include only the period of the day when short-wave irradiance was greater than 200 W m^{-2}, as measured with a pyranometer at a screen-height of 2 m on a weather station 50 m from the experimental field. This filtering resulted in a Tc data set from three sensors with a total of 3,864 individual data points on 15-min time intervals from 50 to 110 DAP.

Temporal Thermal Distortion During a 60-min Simulated UAV-Based Flight Mission. Each Tc value in the time series of stationary infrared sensor measurements represents a single thermal sensor image acquired with a UAV. This represents a time series of images that would be acquired by a stationary UAV hovering over a fixed position in a field. The assumption is that the fixed-position sensor would capture the change in Tc over time with no spatial Tc variation. This "base" time series collected on a 15-min interval was used to represent the Tc from a single UAV thermal image at the beginning of a multiple image UAV mission used to create an orthomosaic image.

Time series of simulated UAV images, from first to last, representing a UAV thermal mission were created to emulate the time stamp differences associated with individual images in UAV missions of 15-, 30-, 45-, and 60-min flight durations. The duration of the flight, 15, 30, 45, or 60 min, indicated the difference in the timestamp between the first image and last image in a UAV mission. The delayed time series are thus referred to as Δ 15 min, Δ 30 min, Δ 45 min, and Δ 60 min.

To investigate the suitability of a solar noon (1345-1353 h from June to August for the experiment site) flight window for thermal flights, pre- and post-solar noon flight windows were included in the analysis. Flight windows for analysis were pre-solar (1030-1230 h), solar (1230-1430 h), and post-solar (1430-1630 h) noon. In subsequent usage the three flight windows (2-h duration) will be referred to in relation to the starting time: 1030, 1230, and 1430 h.

Calculation of Temporal Thermal Distortion for 15, 30, 45, and 60 min. To simulate the change in temperature between images in a UAV mission, changes in Tc were calculated. Two calculations were made to create a new time series of the changes in Tc over time (ΔT). The first calculation was to account for the change in Tc over a particular time period (ΔT). The ΔT was calculated by subtracting the temperature at time 00:00:00 from the temperature from the last image in the time period. For example, the 1030 h Tc value was subtracted from the 1045 h Tc value to give a ΔT for 1045 h. This was repeated with the 1030 h Tc using the 1045, 1100, and 1115 h temperature points. Given that temperature increases in the morning and decreases in the afternoon, the second calculation was to obtain the absolute value of the change in Tc (ΔT). The use of the absolute value of the ΔTs created a new dataset of ΔTs where the change in temperature was always positive and thus could be compared to each other.

Summary of Averages of ΔTs for Each Flight Window. To determine the average change in temperature over 15-, 30-, 45-, and 60-min UAV missions, across the 60-d evaluation period, the resulting ΔTs were binned into the following time windows: 1030-1230, 1230-1430, and 1430-1630 h. As an example, for the 1030 h flight window the 1030, 1045, 1100, 1115, 1130, 1145, 1200, 1215, and 1230 h ΔTs were selected and the averages and standard deviations were calculated for 15-, 30-, 45-, and 60-min periods across low, medium, and high irrigation treatments. The results of the calculations are given in Table 1.

Table 1. Matrix of time-related canopy temperature artifacts, expressed as temporal thermal distortion in °C, for the three irrigation treatments, flight durations (min), and three flight windows (1030–1230, 1230–1430, and 1430–1630 h) over 60 d

	Irrigation Treatment											
	Low				Medium				High			
	Flight Duration (min)											
	15	30	45	60	15	30	45	60	15	30	45	60
Flight Window	Temporal Thermal Distortion (°C)											
1030 h	0.9	1.6	2.2	2.8	0.6	1.0	1.4	1.8	0.7	0.9	1.6	1.4
1230 h	0.7	1.0	1.2	1.5	0.6	0.8	0.9	1.3	0.6	0.7	0.8	0.9
1430 h	0.7	1.0	1.3	1.6	0.6	0.8	0.9	1.1	0.5	0.6	0.8	0.9
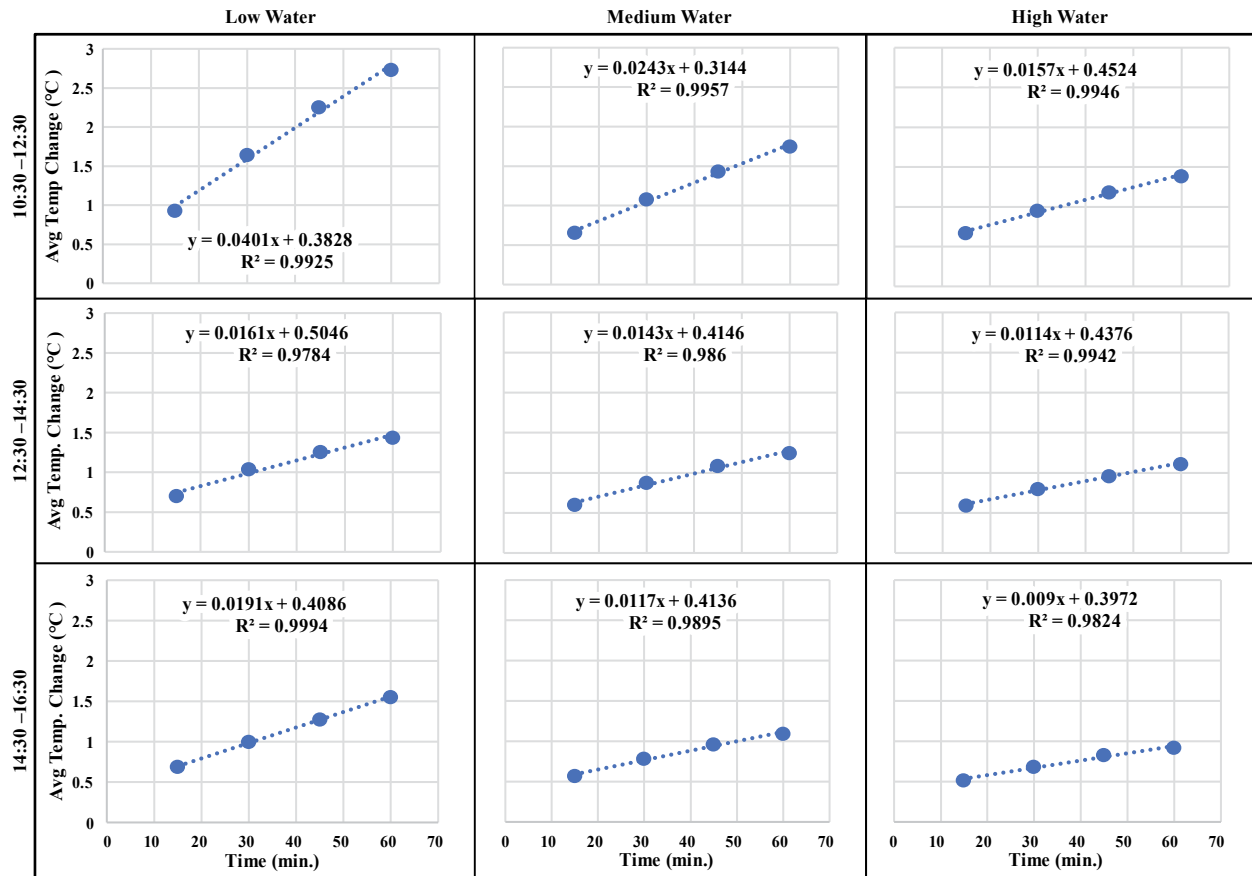
Figure 1. Average changes in temperature on 15-min intervals over the 1-h intervals for the 1030, 1230, and 1430 h simulated flight times. The equations were used to interpolate 1-min data used in Figs. 3 and 4

Modeling of Temperature Changes Across Flight Windows for Irrigation Treatments. We modeled the artifact on a 1-min time interval. The 15-min Tc values were averaged across 56 d and the absolute differences were used to interpolate Tc estimates on a 1-min interval by linear regression. The interpolation resulted in R^2 values ranging from 0.978 to 0.999 that were sufficient for the modeling effort (Figure 1).

RESULTS AND DISCUSSION

Research on temporal changes of Tc in relation to the duration of drone flights and subsequent composition of orthomosaic images is scarce (Kassim et al., 2022; Mesas-Carrascosa et al., 2018; Perich et al., 2020). Specifically, we were unable to find any publications on how to correct thermal images composed from Tc that does not remain constant and is measured with drones. Thus, our results are the first to document how this change in Tc can result in error.

Seasonal Canopy Temperature Patterns. The daily patterns of temperature vary both diurnally and

seasonally in a broad and predictable manner. Fig. 2a shows the seasonal average Tc as a function of the three irrigation treatments for the period from 1000-1800 h over the 60-d study period. Canopy temperature from the three irrigation treatments shows an increase in Tc with declining water status (e.g., at 1400 h a temperature of ~28 °C for the high, ~32 °C for the medium, and ~35 °C for the low irrigation treatments). The three boxes superimposed on the figure represent the 1030, 1230, and 1430 h flight windows.

The rate of change of Tc, in relation to the flight duration, determines the magnitude of the time-related Tc artifacts. Figure 2b shows the rate of change of Tc as the derivative of the absolute values of the diurnal Tc values for the three irrigation treatments. These results demonstrate how Tc stability varies over the course of a day and how the water status of the crop alters that stability. The rate of change of Tc varies continuously over the day in each of the irrigation treatments. In general, the Tc in the high irrigation treatment was more stable, that is, derivative values are lower, than in the medium

or the low irrigation treatments. These results (Fig. 2a and 2b) demonstrate that both time of day and crop water status determine the magnitude of the thermal artifacts in UAV-based Tc measurements that involve multiple images. The influence of time of day and crop water status on the temporal thermal variation was modeled and analyzed using simulations of UAV missions. Crop water status is addressed by analysis of Tc data for three irrigation treatments. Time of day effects on Tc artifacts were assessed in terms of flight windows representing flight periods during a day.
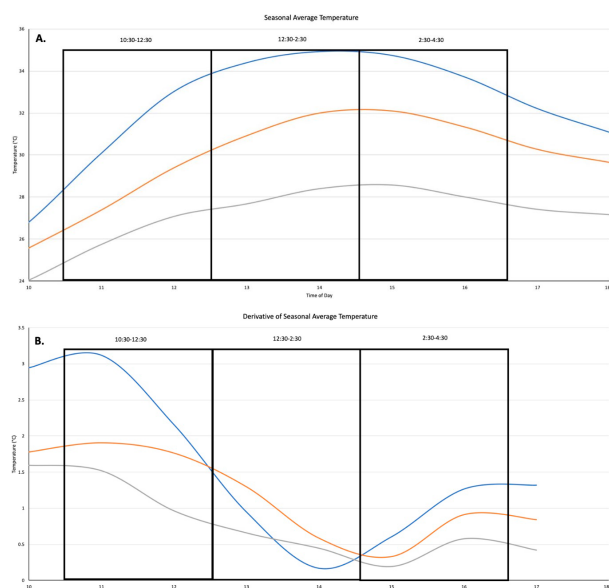

Figure 2. (A) Distribution of average canopy temperatures between 1000 and 1800 h for the 60-d study period for all treatments. (B) Derivative of absolute values for the diurnal canopy temperature data for all treatments. The grey, orange, and blue lines represent high, medium, and low irrigation treatments, respectively. The three boxes superimposed on the figures represent the 1030, 1230, and 1430 h flight windows.

Time-Related Canopy Temperature Artifacts. Table 1 shows the time-related Tc artifacts in relation to flight window, water status (irrigation treatment), and flight duration for the 60-d study interval (50-110 DAP). Canopy temperature artifacts refer to thermal distortion as given in Table 1. The Tc artifacts vary with flight duration, water level, and flight window in an interactive manner. For example, in the 1030 h flight window, the time-related Tc artifact increases from 0.9 to 2.8 °C with increasing flight duration. In general, time-related Tc artifacts decrease with increasing irrigation. For example, 2.8 °C at low irrigation to 1.4 °C for a high irrigation with a 60-min flight

duration. The 1030 h flight window had the highest artifact values with 1230 and 1430 h having lower Tc artifacts of 0.1 °C in most cases. The time-related Tc artifacts are lowest for 15-min flight durations across all flight windows and irrigation treatments (0.5-0.9 °C).

Visualizations of Temporal Thermal Distortion. To visualize the thermal distortion in a more continuous manner, the measured Tc at 15-min intervals was interpolated to 1-min values (see Materials and Methods: Modeling of Temperature Changes Across Flight Windows for Irrigation Treatments). Figure 3 shows the magnitude of thermal distortion (°C) induced by sequential 1-min intervals between Tc measurements with fixed IRTs in cotton over the 60-d study period. Thermal distortion is shown for each of the three daily flight windows (1030, 1230, and 1430 h) across three irrigation treatments. Across all three flight windows, the thermal distortion decreases with increasing irrigation treatment. The thermal distortion is highest in the early flight window and is similar in the middle and late flight windows.

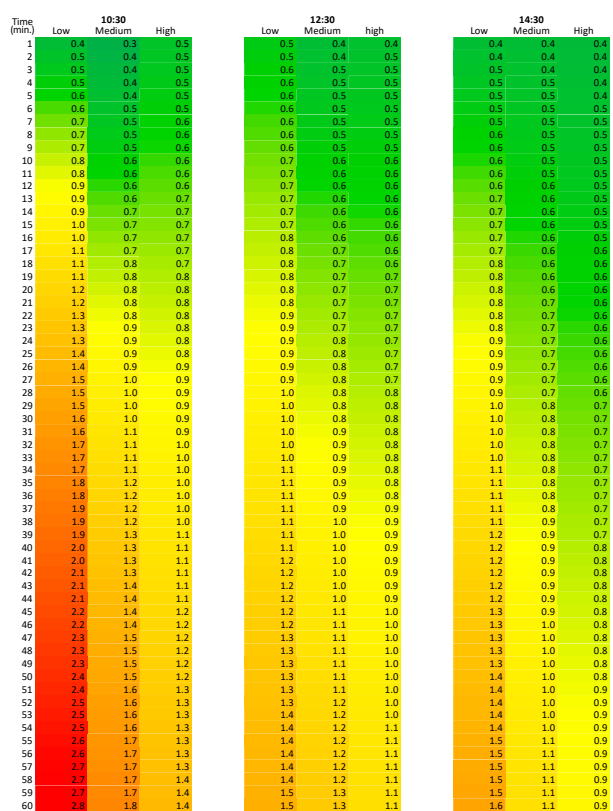| Time (min.)	10:30 Low	Medium	High	12:30 Low	Medium	high	14:30 Low	Medium	High
1	0.4	0.3	0.5	0.5	0.4	0.4	0.4	0.4	0.4
2	0.5	0.4	0.5	0.5	0.4	0.5	0.4	0.4	0.4
3	0.5	0.4	0.5	0.5	0.5	0.5	0.5	0.4	0.4
4	0.5	0.4	0.5	0.6	0.5	0.5	0.5	0.5	0.4
5	0.6	0.4	0.5	0.6	0.5	0.5	0.5	0.5	0.4
6	0.6	0.5	0.5	0.6	0.5	0.5	0.5	0.5	0.5
7	0.7	0.5	0.6	0.6	0.5	0.5	0.5	0.5	0.5
8	0.7	0.5	0.6	0.6	0.5	0.5	0.6	0.5	0.5
9	0.7	0.5	0.6	0.6	0.5	0.5	0.6	0.5	0.5
10	0.8	0.6	0.6	0.7	0.6	0.6	0.6	0.5	0.5
11	0.8	0.6	0.6	0.7	0.6	0.6	0.6	0.5	0.5
12	0.9	0.6	0.6	0.7	0.6	0.6	0.6	0.6	0.5
13	0.9	0.6	0.7	0.7	0.6	0.6	0.7	0.6	0.5
14	0.9	0.7	0.7	0.7	0.6	0.6	0.7	0.6	0.5
15	1.0	0.7	0.7	0.7	0.6	0.6	0.7	0.6	0.5
16	1.0	0.7	0.7	0.8	0.6	0.6	0.7	0.6	0.5
17	1.1	0.7	0.7	0.8	0.7	0.6	0.7	0.6	0.6
18	1.1	0.8	0.7	0.8	0.7	0.6	0.8	0.6	0.6
19	1.1	0.8	0.8	0.8	0.7	0.7	0.8	0.6	0.6
20	1.2	0.8	0.8	0.8	0.7	0.7	0.8	0.6	0.6
21	1.2	0.8	0.8	0.8	0.7	0.7	0.8	0.7	0.6
22	1.3	0.8	0.8	0.9	0.7	0.7	0.8	0.7	0.6
23	1.3	0.9	0.8	0.9	0.7	0.7	0.8	0.7	0.6
24	1.3	0.9	0.8	0.9	0.8	0.7	0.9	0.7	0.6
25	1.4	0.9	0.8	0.9	0.8	0.7	0.9	0.7	0.6
26	1.4	0.9	0.9	0.9	0.8	0.7	0.9	0.7	0.6
27	1.5	1.0	0.9	0.9	0.8	0.7	0.9	0.7	0.6
28	1.5	1.0	0.9	1.0	0.8	0.8	0.9	0.7	0.6
29	1.5	1.0	0.9	1.0	0.8	0.8	1.0	0.8	0.7
30	1.6	1.0	0.9	1.0	0.8	0.8	1.0	0.8	0.7
31	1.6	1.1	0.9	1.0	0.9	0.8	1.0	0.8	0.7
32	1.7	1.1	1.0	1.0	0.9	0.8	1.0	0.8	0.7
33	1.7	1.1	1.0	1.0	0.9	0.8	1.0	0.8	0.7
34	1.7	1.1	1.0	1.1	0.9	0.8	1.1	0.8	0.7
35	1.8	1.2	1.0	1.1	0.9	0.8	1.1	0.8	0.7
36	1.8	1.2	1.0	1.1	0.9	0.8	1.1	0.8	0.7
37	1.9	1.2	1.0	1.1	0.9	0.9	1.1	0.8	0.7
38	1.9	1.2	1.0	1.1	1.0	0.9	1.1	0.9	0.7
39	1.9	1.3	1.1	1.1	1.0	0.9	1.2	0.9	0.7
40	2.0	1.3	1.1	1.1	1.0	0.9	1.2	0.9	0.8
41	2.0	1.3	1.1	1.2	1.0	0.9	1.2	0.9	0.8
42	2.1	1.3	1.1	1.2	1.0	0.9	1.2	0.9	0.8
43	2.1	1.4	1.1	1.2	1.0	0.9	1.2	0.9	0.8
44	2.1	1.4	1.1	1.2	1.0	0.9	1.2	0.9	0.8
45	2.2	1.4	1.2	1.2	1.1	1.0	1.3	0.9	0.8
46	2.2	1.4	1.2	1.2	1.1	1.0	1.3	1.0	0.8
47	2.3	1.5	1.2	1.3	1.1	1.0	1.3	1.0	0.8
48	2.3	1.5	1.2	1.3	1.1	1.0	1.3	1.0	0.8
49	2.3	1.5	1.2	1.3	1.1	1.0	1.3	1.0	0.8
50	2.4	1.5	1.2	1.3	1.1	1.0	1.4	1.0	0.8
51	2.4	1.6	1.3	1.3	1.1	1.0	1.4	1.0	0.9
52	2.5	1.6	1.3	1.3	1.2	1.0	1.4	1.0	0.9
53	2.5	1.6	1.3	1.4	1.2	1.0	1.4	1.0	0.9
54	2.5	1.6	1.3	1.4	1.2	1.1	1.4	1.0	0.9
55	2.6	1.7	1.3	1.4	1.2	1.1	1.5	1.1	0.9
56	2.6	1.7	1.3	1.4	1.2	1.1	1.5	1.1	0.9
57	2.7	1.7	1.3	1.4	1.2	1.1	1.5	1.1	0.9
58	2.7	1.7	1.4	1.4	1.2	1.1	1.5	1.1	0.9
59	2.7	1.7	1.4	1.5	1.3	1.1	1.5	1.1	0.9
60	2.8	1.8	1.4	1.5	1.3	1.1	1.6	1.1	0.9

Figure 3. Modeled heat map representing temperature distortion (°C) for each minute of a 60-min UAV flight. Thermal distortion is shown by minute in relation to flight window (1030, 1230, and 1430 h), flight duration (0 to 60 min), and irrigation treatment (low, medium, and high).

10:30 — Low

00:01	00:30	00:31	00:60
0.4	1.6	1.6	2.8
0.5	1.5	1.7	2.7
0.5	1.5	1.7	2.7
0.5	1.5	1.7	2.7
0.6	1.4	1.8	2.6
0.6	1.4	1.8	2.6
0.7	1.3	1.9	2.5
0.7	1.3	1.9	2.5
0.7	1.3	1.9	2.5
0.8	1.2	2.0	2.4
0.8	1.2	2.0	2.4
0.9	1.1	2.1	2.3
0.9	1.1	2.1	2.3
0.9	1.1	2.1	2.3
00:15 1.0	00:16 1.0	00:45 2.2	00:46 2.2

(Arrows in the first panel indicate the boustrophedonic flight path: down, up, down, up.)

10:30 — Medium

00:01	00:30	00:31	00:60
0.3	1.0	1.1	1.8
0.4	1.0	1.1	1.7
0.4	1.0	1.1	1.7
0.4	1.0	1.2	1.7
0.4	0.9	1.2	1.7
0.5	0.9	1.2	1.6
0.5	0.9	1.2	1.6
0.5	0.9	1.3	1.6
0.5	0.8	1.3	1.6
0.6	0.8	1.3	1.5
0.6	0.8	1.3	1.5
0.6	0.8	1.4	1.5
0.6	0.8	1.4	1.5
0.7	0.7	1.4	1.5
00:15 0.7	00:16 0.7	00:45 1.4	00:46 1.4

10:30 — High

00:01	00:30	00:31	00:60
0.5	0.9	0.9	1.4
0.5	0.9	1.0	1.4
0.5	0.9	1.0	1.4
0.5	0.9	1.0	1.3
0.5	0.9	1.0	1.3
0.6	0.8	1.0	1.3
0.6	0.8	1.0	1.3
0.6	0.8	1.1	1.3
0.6	0.8	1.1	1.3
0.6	0.8	1.1	1.2
0.7	0.7	1.1	1.2
0.7	0.7	1.1	1.2
0.7	0.7	1.1	1.2
0.7	0.7	1.1	1.2
00:15 0.7	00:16 0.7	00:45 1.2	00:46 1.2

12:30 — Low

00:01	00:30	00:31	00:60
0.5	1.0	1.0	1.5
0.5	1.0	1.0	1.5
0.6	1.0	1.0	1.4
0.6	0.9	1.1	1.4
0.6	0.9	1.1	1.4
0.6	0.9	1.1	1.4
0.6	0.9	1.1	1.4
0.6	0.9	1.1	1.3
0.6	0.9	1.1	1.3
0.7	0.8	1.1	1.3
0.7	0.8	1.2	1.3
0.7	0.8	1.2	1.3
0.7	0.8	1.2	1.3
0.7	0.8	1.2	1.3
00:15 0.7	00:16 0.8	00:45 1.2	00:46 1.2

12:30 — Medium

00:01	00:30	00:31	00:60
0.4	0.8	0.9	1.3
0.4	0.8	0.9	1.3
0.5	0.8	0.9	1.2
0.5	0.8	0.9	1.2
0.5	0.8	0.9	1.2
0.5	0.8	0.9	1.2
0.5	0.7	1.0	1.2
0.5	0.7	1.0	1.2
0.6	0.7	1.0	1.1
0.6	0.7	1.0	1.1
0.6	0.7	1.0	1.1
0.6	0.7	1.0	1.1
0.6	0.7	1.0	1.1
0.6	0.7	1.0	1.1
00:15 0.6	00:16 0.6	00:45 1.1	00:46 1.1

12:30 — High

00:01	00:30	00:31	00:60
0.4	0.8	0.8	1.1
0.5	0.8	0.8	1.1
0.5	0.8	0.8	1.1
0.5	0.7	0.8	1.1
0.5	0.7	0.8	1.1
0.5	0.7	0.8	1.1
0.5	0.7	0.9	1.0
0.5	0.7	0.9	1.0
0.6	0.7	0.9	1.0
0.6	0.7	0.9	1.0
0.6	0.7	0.9	1.0
0.6	0.6	0.9	1.0
0.6	0.6	0.9	1.0
0.6	0.6	0.9	1.0
00:15 0.6	00:16 0.6	00:45 1.0	00:46 1.0

14:30 — Low

00:01	00:30	00:31	00:60
0.4	1.0	1.0	1.6
0.4	1.0	1.0	1.5
0.5	0.9	1.0	1.5
0.5	0.9	1.1	1.5
0.5	0.9	1.1	1.5
0.5	0.9	1.1	1.5
0.6	0.8	1.1	1.4
0.6	0.8	1.2	1.4
0.6	0.8	1.2	1.4
0.6	0.8	1.2	1.4
0.6	0.8	1.2	1.3
0.7	0.8	1.2	1.3
0.7	0.7	1.2	1.3
00:15 0.7	00:16 0.7	00:45 1.3	00:46 1.3

14:30 — Medium

00:01	00:30	00:31	00:60
0.4	0.8	0.8	1.1
0.4	0.8	0.8	1.1
0.4	0.7	0.8	1.1
0.5	0.7	0.8	1.1
0.5	0.7	0.8	1.1
0.5	0.7	0.8	1.0
0.5	0.7	0.9	1.0
0.5	0.7	0.9	1.0
0.5	0.6	0.9	1.0
0.6	0.6	0.9	1.0
0.6	0.6	0.9	1.0
0.6	0.6	0.9	1.0
00:15 0.6	00:16 0.6	00:45 0.9	00:46 1.0

14:30 — High

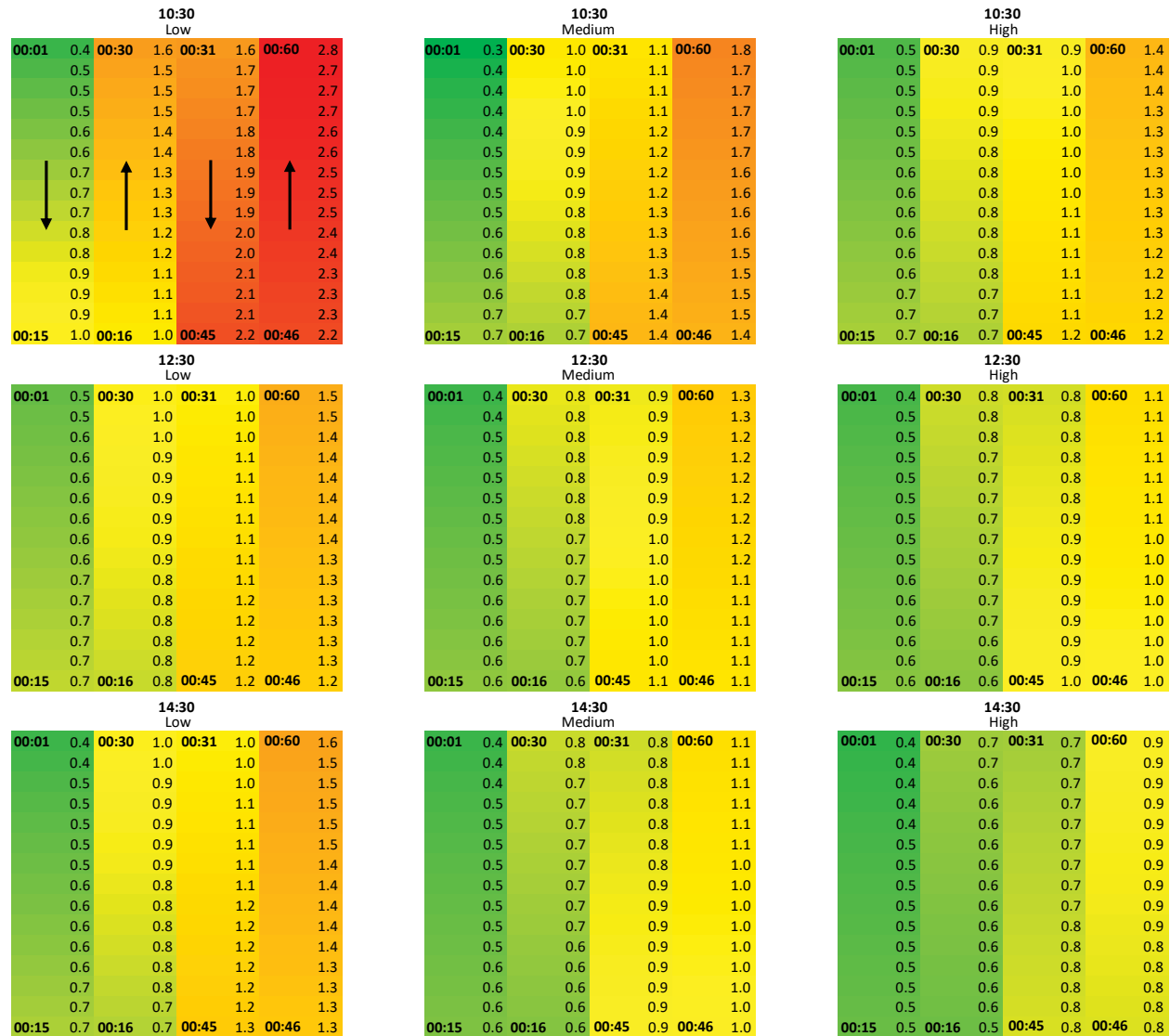| 00:01	00:30	00:31	00:60
0.4	0.7	0.7	0.9
0.4	0.7	0.7	0.9
0.4	0.6	0.7	0.9
0.4	0.6	0.7	0.9
0.4	0.6	0.7	0.9
0.5	0.6	0.7	0.9
0.5	0.6	0.7	0.9
0.5	0.6	0.7	0.9
0.5	0.6	0.8	0.9
0.5	0.6	0.8	0.8
0.5	0.6	0.8	0.8
0.5	0.6	0.8	0.8
00:15 0.5	00:16 0.5	00:45 0.8	00:46 0.8

Figure 4. The time-related canopy temperature artifacts in a simulated orthomosaic heat map showing the data from Fig. 2 in the format of a heat map that would be produced during a UAV thermal mission according to a boustrophedonic (lawnmower) pattern. Each block represents the temperature distortion (°C) for each minute of a 60-min UAV flight. Thermal distortion is shown by minute in relation to flight window (1030, 1230, and 1430 h), flight duration (0 to 60 min), and irrigation treatment (low, medium, and high).

The temporal thermal distortion shows a complex interaction between the flight window and water status of the crop, which comprise two important aspects of UAV thermal missions. As previously noted, a key assumption in agronomic photogrammetry is that the variable of interest does not change during the period of measurement. Under this constraint in an orthomosaic image the spatial relationships remain intact; however, in the instance of Tc measurements, the temporal relations are not necessarily related to the spatial component. Figure 4 is the thermal distortion from Fig. 3 arranged into a simulated orthomosaic heat map that would be produced during a 60-min UAV thermal mission according to a boustrophedonic (lawnmower) flight pattern.

A "lawnmower" flight pattern is shown with arrows indicating the flight path of the UAV (sequence of images over time). From one image to the next, Tc changes and that change is shown as the Tc difference from one image to the next. If the Tc did not change over the duration of the flight, all the Tc values would be equal, and the panel would be a single color. The time required to collect all the images determines the Tc differences among the collection of cells and the pattern of the flight determines the distribution of the Tc distortion across the composite image. In the lawnmower pattern, cells (images) that are spatially adjacent might not be temporally adjacent in the composite representation. For example, im-

age #15 and image #16 are spatially adjacent, their timestamps differ by only 1 min. and the thermal distortion between the pair is 0 °C; whereas image #1 and image #30 are spatially adjacent, the image timestamps differ by 30 min and the thermal distortion between the pair differs by 1.2 °C. Thus, in the composite image, thermal distortion does not map to spatial position.

Broadly, the 1030 h flight window has the greatest thermal distortion across all irrigation levels compared to the 1230 and 1430 h flight windows. Across all flight windows, increasing irrigation levels stabilizes the Tc across a 60-min flight duration. Knowledge of the spatial thermal distortion in the composite image might prove helpful in comparisons of Tc within a composite thermal image.

SUMMARY

The magnitude of the time-related Tc artifacts is a function of the change in Tc over the measurement period (flight duration). The stability of Tc is a result of several interacting variables, mainly time of day and crop water status for arid regions but can also be affected by changes in solar radiation due to cloud cover and intermittent clouds in temperate and tropical regions (Mahan et al., 2010; Wanjura et al., 2006). Although there will be time-related Tc artifacts present in crop thermal images from UAV platforms under most flight conditions, the magnitude of the effect is difficult to estimate or measure (Chang et al., 2020; Mesas-Carrascosa et al., 2018). The magnitude of time-related Tc artifacts within a composited thermal orthomosaic image should be considered with respect to the thermal resolution required for the analysis. The detection of a 0.5 °C difference in an image would probably be more affected by flight-induced variation than the detection of a 5 °C difference (Mesas-Carrascosa et al., 2018). The measured time-related Tc artifacts vary from negligible (< 0.5 °C) to potentially significant (> 2.5 °C) (Wanjura et al., 2002, 2006).

Given the sources of thermal variability, the mitigation of time-related Tc artifacts in UAV thermal missions can be accomplished to some extent. The specifics will vary regionally, and these results are limited in some extent to the environment. Within the thermal environment of this study several adjustments would help reduce time-related Tc artifacts: 1) reduction of flight duration (less thermal change between first and last image in a collection); 2) flying after solar noon; and 3) avoiding and/or being aware of plant water deficits. The authors propose that this method can be used to extract the magnitude of time-related Tc artifacts and potential mitigation in other climatic regions. Given an orthomosaic heat-map image as a desired product, care should be taken to assure that these artifacts are considered.

The sources of time-related Tc artifacts analyzed in this study include flight duration, daily flight windows, and crop water status. The result of this analysis provided estimates of the magnitude of the time-related Tc artifacts that could be expected from the crop Tc measurements collected with a thermal sensor mounted on a UAV. The time-related Tc artifacts that are modeled in this study represent a physical reality. The temperature artifacts that might be experienced during any particular day could be highly variable given that day's temperature (Wanjura and Mahan, 1994; Wanjura et al., 2002, 2006). In humid regions, Tc can change rapidly due to changes in solar radiation caused by cloud cover. Intermittent cloud cover during a thermal UAV flight would only cause further exaggeration of the thermal artifact. For a given crop target, imaged in a specified flight window, with a specified flight duration, the time-related Tc artifacts within an orthomosaic image could be worse than predicted by this analysis but likely not better.

Based on this the analysis several points could be useful for improving the utility of UAV-based thermal imaging in crops.

1) Thermal UAV missions should be kept as short as possible. This will limit the area that can be imaged but perhaps improve image quality.
2) A post-solar noon flight window will generally reduce time-related Tc artifacts.
3) Variations in crop water status were the single largest source of time-related Tc artifacts and should be known if possible.
4) An orthomosaic thermal image can have inherent time-related Tc artifacts of the displayed temperature.

DISCLAIMER

Mention of trade names or commercial products in this publication is solely for the purpose of providing specific information and does not imply recommendation or endorsement by the U.S. Department of Agriculture. USDA is an equal opportunity provider and employer.

REFERENCES

Andrade-Sanchez, P., M.A. Gore, J.T. Heun, K.R. Thorp, E. A.N. Carmo-Silva, French, M.E. Salvucci, and J.W. White. 2014. Development and evaluation of a field-based high-throughput phenotyping platform. Functional Plant Biol. 41:68–79. https://doi.org/10.1071/FP13126

Bacsa, C.M., R.M. Martorillas, L.P. Balicanta, and A.M. Ta-mondong. 2019. Correlation of UAV-Based Multispectral Vegetation Indices and Leaf Color Chart Observations for Nitrogen Concentration Assessment on Rice Crops. The International Archives of the Photogrammetry, Remote Sensing and Spatial Information Sciences, Volume XLII-4/W19, PhilGEOS x GeoAdvances, Manila, Philippines. https://doi.org/10.5194/isprs-archives-XLII-4-W19-31-2019

Berni, J.A.J., P.J. Zarco-Tejada, G. Sepulcre-Cantó, E. Fereres, and F. Villalobos. 2009a. Mapping canopy conductance and CWSI in olive orchards using high resolution thermal remote sensing imagery. Remote Sens. Environ. 113(11):2380–2388. https://doi.org/10.1016/j.rse.2009.06.018

Berni, J.A.J., P.J. Zarco-Tejada, L. Suarez, and E. Fer-eres. 2009b. Thermal and narrowband multispectral remote sensing for vegetation monitoring from an unmanned aerial vehicle. IEEE Trans. Geosci. Remote Sens. 47(3):722–738. https://doi.org/10.1109/TGRS.2008.2010457.

Chang, A., J. Jung, M.M. Maeda, J.A. Landivar, H.D.R. Carv-alho, and J. Yeom. 2020. Measurement of cotton canopy temperature using radiometric thermal sensor mounted on the unmanned aerial vehicle (UAV). J. Sensors. 2020:8899325. https://doi.org/10.1155/2020/8899325

Chu, T., M.J. Starek, M.J. Brewer, S.C. Murray, and L.S. Pruter. 2018. Characterizing canopy height with UAS structure-from-motion photogrammetry–results analysis of a maize field trial with respect to multiple factors. Remote Sens. Letters, 9:753–762. https://doi.org/10.1080/2150704X.2018.1475771

Colomina, I., and P. Molina. 2014. Unmanned aerial systems for photogrammetry and remote sensing: A review. ISPRS J. Photogrammetry and Remote Sens. 92:79–97. https://doi.org/10.1016/j.isprsjprs.2014.02.013

Dandois, J.P., M. Baker, M. Olano, G.G. Parker, and E.C. Ellis. 2017. What is the point? Evaluating the structure, color, and semantic traits of computer vision point clouds of vegetation. Remote Sens. 9:355. https://doi.org/10.3390/rs9040355

Gerbermann, A.H., J.A. Cuellar, and C.L. Wiegand. 1976. Ground cover estimated from aerial photographs. Photogrammetric Engineering and Remote Sens. 42:551–556.

Gil-Docampo, M.L., M. Arza-García, J. Ortiz-Sanz, S. Mar-tínez-Rodríguez, J.L. Marcos-Robles, and L.F. Sánchez-Sastre. 2020. Above-ground biomass estimation of arable crops using UAV-based SfM photogrammetry. Geocarto Internat. 35:687–699. https://doi.org/10.1080/10106049.2018.1552322

Gonzalez-Dugo, V., P.J. Zarco-Tejada, E. Nicolás, P.A. Nortes, J.J. Alarcon, D.S. Intrigliolo, and E. Fereres. 2013. Using high resolution UAV thermal imagery to assess the variability in the water status of five fruit tree species within a commercial orchard. Precision Agric. 14(6):660–678. https://doi.org/10.1007/s11119-013-9322-9

Jung, J., M.M. Maeda, A. Chang, J.A. Landivar, J. Yeom, and J. McGinty. 2018. Unmanned aerial system assisted framework for the selection of high yielding cotton genotypes. Comput. Electron. Agric. 152:74–81. https://doi.org/10.1016/j.compag.2018.06.051

Kassim Y.B., R. Oteng-Frimpong, D.K. Puozaa, E.K. Sie, M. Abdul Rasheed, I. Abdul Rashid, A. Danquah, D.A. Akogo, J. Rhoads, D. Hoisington, M.D. Burow, and M. Balota. 2022 High-throughput plant phenotyping (HTPP) in resource-constrained research programs: a working example in Ghana. Agron. 12(11):2733. https://doi.org/10.3390/agronomy12112733

Mahan, J.R., J.J. Burke, D.F. Wanjura, and D.R. Upchurch. 2005. Determination of temperature and time thresh-olds for BIOTIC irrigation of peanut on the Southern High Plains of Texas. Irrig. Sci. 23:145–152. https://doi.org/10.1007/s00271-005-0102-9

Mahan, J.R., W. Conaty, J. Neilsen, P. Payton, and S.B. Cox. 2010. Field performance in agricultural settings of a wireless temperature monitoring system based on a low-cost infrared sensor. Comput. Electron. Agric. 71(2):176–181. https://doi.org/10.1016/j.compag.2010.01.005

Matese, A., S.F. Di Gennaro, and A. Berton. 2017. Assessment of a canopy height model (CHM) in a vineyard using UAV-based multispectral imaging. Internat. J. Remote Sens. 38:2150–2160. https://doi.org/10.1080/01431161.2016.1226002

Mesas-Carrascosa F.-J., F. Pérez-Porras, J.E. Meroño de Lar-riva, C. Mena Frau, F. Agüera-Vega, F. Carvajal-Ramírez, P. Martínez-Carricondo, and A. García-Ferrer. 2018. Drift correction of lightweight microbolometer thermal sensors on-board unmanned aerial vehicles. Remote Sens. 10(4):615. https://doi.org/10.3390/rs10040615

Murakami, T., M. Yui, and K. Amaha. 2012. Canopy height measurement by photogrammetric analysis of aerial images: application to buckwheat (*Fagopyrum esculentum* Moench) lodging evaluation. Computers and Electronics in Agric. 89:70–75.

Pabuayon-Irish, L.B., Y. Sun, W. Guo, and G.L. Ritchie. 2019. High-throughput phenotyping in cotton: a review. J. Cotton Res. 2:8. https://doi.org/10.1186/s42397-019-0035-0

Perich, G., A. Hund, J. Anderegg, L. Roth, M.P. Boer, A. Walter, F. Liebisch, and H. Aasen. 2020. Assessment of multi-image unmanned aerial vehicle based high-throughput field phenotyping of canopy temperature. Front. Plant Sci. 11:150. https://doi.org/ 10.3389/fpls.2020.00150

Pratap, A., R. Tomar, J. Kumar, V.R. Pandey, S. Mehandi, and P.K. Katiyar. 2015. High-throughput plant phenotyping platforms, pp. 285–296 *In* Kumar J., Pratap A., Kumar S. (eds.), Phenomics in Crop Plants: Trends, Options and Limitations. Springer, New Delhi. https://doi.org/10.1007/978-81-322-2226-2_19

Raeva, P., J. Šedina, and A. Dlesk. 2018. UAV photogrammetry techniques for precision agriculture, pp. 842–855 *In* Proc. 7th Intern. Conf. on Cartography and GIS, 18-23 June 2018, Sozopol, Bulgaria. Bulgarian Cartographic Association, Sofia, Bulgaria. Available online at https://iccgis2018.cartography-gis.com/7ICCGIS_Proceedings/7_ICCGIS_2018%20(93).pdf (verified 26 Aug. 2023).

Roth, L., and B. Streit. 2018. Predicting cover crop biomass by lightweight UAS-based RGB and NIR photography: an applied photogrammetric approach. Precision Agric. 19:93–114. https://doi.org/10.1007/s11119-017-9501-1

Vadivambal, R., and D.R. Jayas. 2011. Applications of thermal imaging in agriculture and food industry—a review. Food Bioprocess Tech. 4(2):186–199. https://doi.org/10.1007/s11947-010-0333-5

Walter, J., J. Edwards, G. McDonald, and H. Kuchel. 2018. Photogrammetry for the estimation of wheat biomass and harvest index. Field Crops Res. 216:165–174.

Wanjura, D.F., and J.R. Mahan. 1994. Thermal environment of cotton irrigated using canopy temperature. Irrig. Sci. 14:199–205. https://doi.org/10.1007/BF00190191

Wanjura, D.F., D.R. Upchurch, and J.R. Mahan. 1995. Control of irrigation scheduling using temperature-time thresholds Trans. ASAE. 38:403–409.

Wanjura, D.F., D.R. Upchurch, and J.R. Mahan. 2006. Behavior of temperature-based water stress indicators in BIOTIC-controlled irrigation. Irrig. Sci. 24:223–232. https://doi.org/10.1007/s00271-005-0021-9

Wanjura, D.F., D.R. Upchurch, J.R. Mahan, and J.J. Burke. 2002. Cotton yield and applied water relationships under drip irrigation. Agric. Water Manage. 55(3):217–237. https://doi.org/10.1016/S0378-3774(01)00175-5

Weiss, M., F. Jacob, and G. Duveiller. 2020. Remote sensing for agricultural applications: A meta review. Remote Sens. Environ. 236:111402. https://doi.org/10.1016/j.rse.2019.111402

Zarco-Tejada, P.J., V. González-Dugo, and J.A.J. Berni. 2012. Fluorescence, temperature and narrow-band indices acquired from a UAV platform for water stress detection using a microhyperspectral imager and a thermal camera. Remote Sens. Environ. 117:322–337. https://doi.org/10.1016/j.rse.2011.10.007

Zhang, C., and J.M. Kovacs. 2012. The application of small unmanned aerial systems for precision agriculture: A review. Precision Agric. 13:693–712. https://doi.org/10.1007/s11119-012-9274-5